

Project report

Course : Introduction to Finite Element Modeling in Geosciences

Sthavishtha Bhopalam Rajakumar
ETH Zürich, Switzerland

September 14, 2019

Abstract

The current report details the numerical solutions of the following two-dimensional problems using finite element methods : transient heat diffusion, elasticity and flow in a dam break (Stokes flow). Successful code verification using the method of manufactured solutions has also been performed for the first two problems. On the application part, the phenomenon of viscous fingering instability occurring in porous media has been simulated using the developed code framework.

1 2D diffusion equation

This section studies a two-dimensional transient diffusion equation, the conservation equation of which can be given by,

$$\frac{\partial T}{\partial t} = k \left(\frac{\partial^2 T}{\partial x^2} + \frac{\partial^2 T}{\partial y^2} \right) + S \quad (1)$$

where T , k , S refer to the temperature, thermal diffusivity and source terms (heat sources/sinks) respectively.

The corresponding set of discrete element equations can be given as,

$$\mathbf{M} \left(\frac{\partial \mathbf{T}}{\partial t} \right) + \mathbf{K} \mathbf{T} = \mathbf{F} \quad (2)$$

where

$$\begin{aligned} \mathbf{M} &= \int \int \mathbf{N}^T \mathbf{N} dx dy \\ \mathbf{K} &= \int \int (\nabla \mathbf{N})^T \mathbf{D} \nabla \mathbf{N} dx dy \\ \mathbf{F} &= \int \int \mathbf{N}^T S dx dy + \int \mathbf{N}^T \mathbf{q} \cdot \mathbf{n} dS \end{aligned} \quad (3)$$

where, \mathbf{N} refer to the shape functions (bilinear or biquadratic), while \mathbf{D} , \mathbf{q} refer to the diffusivity matrix (isotropic, in the current report) and boundary flux terms.

Using a first order explicit approach for time discretization, the above equations can be appropriately rewritten to yield an assembly matrix which can be numerically solved,

$$\begin{aligned} \left(\frac{\mathbf{M}}{\delta t} + \mathbf{K} \right) \mathbf{T}^{n+1} &= \frac{\mathbf{M}}{\delta t} \mathbf{T}^n + \mathbf{F} \\ \mathbf{L} \mathbf{T}^{n+1} &= \mathbf{R} \mathbf{T}^n + \mathbf{F} \end{aligned} \quad (4)$$

To test the code framework in handling heat diffusion problems, a transient setup with zero dirichlet boundary conditions on all boundaries were simulated. For simplicity, source and flux terms in the Eqn. 3 were neglected. Additionally, the temperature was initialized in the form of a gaussian function, $100 \exp [-((x - x_c)^2 + (y - y_c)^2)]$ (x_c , y_c refer to the centres of the domain), and corresponding 3D surface plots and 2D contours subsequently captured with the passage of time. Fig. 1 shows the plots for the corresponding parameters detailed in Table 1. To verify the credibility of the results, the

Parametric variables	Parameters
Domain lengths	1 m (both x & y)
Elements	29 (both x & y)
Thermal diffusivity	0.01 m^2/s (both x & y)
Source terms	0 (both x & y)
Time step	0.2 s

Table 1: Parameters used for simulating 2D transient diffusion

code was tested for both bilinear and biquadratic elements, and 2×2 and 3×3 Gauss quadrature integration points, all of which yielded similar results. For brevity, the simulation results shown here have been obtained on using biquadratic elements and 3×3 Gauss quadrature integration points.

Code verification was performed by employing the method of manufactured solutions, and the L_2 convergence errors noted down with successive grid refinement. For this purpose, the manufactured temperature was chosen to be a function of the form $\sin\left(\frac{\pi x}{L_x}\right) \cos\left(\frac{\pi y}{L_y}\right)$. Substituting this expression into Eqn. 1 yielded $\left(\frac{\pi^2}{L_x^2} + \frac{\pi^2}{L_y^2}\right) \sin\left(\frac{\pi x}{L_x}\right) \cos\left(\frac{\pi y}{L_y}\right)$ as the right hand side terms, which need to be accounted as boundary conditions in the assembly matrix (Eqn. 3). Using bilinear shape functions and 2×2 Gauss quadrature integration points, an order of accuracy equal to 1.9993 was obtained. Additionally, biquadratic shape functions with 2×2 and 3×3 Gauss quadrature integration points respectively yielded an order of accuracy equal to 2.9965 and 2.9994. The obtained convergence plot and numerical solution on using these manufactured equations is shown in Fig. 2. The L_2 convergence errors plotted in Fig. 2 were computed in the form of $\sqrt{(T_{fem} - T_{mms})^2 dV}$, where T_{fem} and T_{mms} respectively refer to the temperatures from the current FEM solution and manufactured equations. From the orders of accuracy reported earlier, it can be seen that 3×3 quadrature points are more accurate than the counterpart 2×2 quadrature points¹. This is not easily discernible in Fig. 2 due to the minute difference between the two and the simplicity of the setup. However, the computed orders of accuracy are consistent with the expected orders of accuracy on using bilinear and biquadratic shape functions, which deems the current code framework to be reliable for subsequent simulations.

As an additional test, the code was tested even when the grid is slightly deformed or perturbed. For this, a small perturbation in the domain center was induced, and the corresponding simulation results captured in Fig. 3. The surface and contour plots are similar to the ones shown in Fig. 1. Additionally, no instabilities in jacobian computation or elemental matrix assembly were observed, which further verifies the credibility of the current code framework.

2 2D elasticity equation

This section studies a solid mechanics problem, to describe the behavior of elastic solids. The conservation equation for the solid displacement can be simply given as,

$$\mathbf{B}^T \mathbf{D} \mathbf{B} \mathbf{e} = 0 \quad (5)$$

which is recovered after eliminating the stresses and strains using known constitutive relations. Here, e refers to the displacement vector, and the matrices \mathbf{D} and \mathbf{B} can be given as,

$$\begin{aligned} \mathbf{B} &= \begin{bmatrix} \frac{\partial}{\partial x} & 0 \\ 0 & \frac{\partial}{\partial y} \\ \frac{\partial}{\partial x} & \frac{\partial}{\partial y} \end{bmatrix} \\ \mathbf{D} &= \frac{E}{(1 + \nu)(1 - 2\nu)} \begin{bmatrix} 1 - \nu & \nu & 0 \\ \nu & 1 - \nu & 0 \\ 0 & 0 & \frac{1}{2}(1 - 2\nu) \end{bmatrix} \\ \mathbf{e} &= \begin{bmatrix} u_x \\ u_y \end{bmatrix} \end{aligned} \quad (6)$$

¹This can also be verified from the convergence errors reported in the text file *L2errors*, in the folder */codes/mms/*

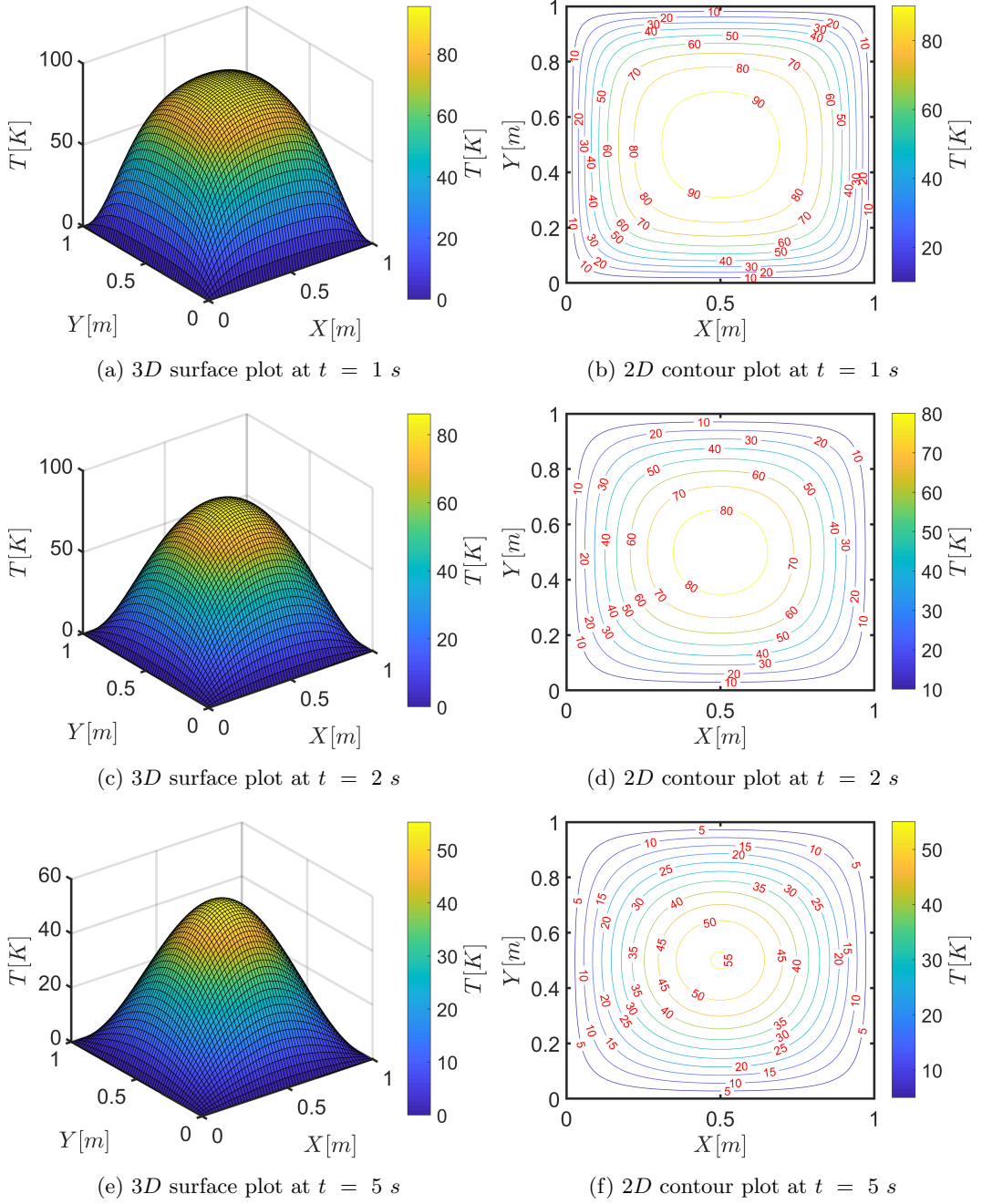


Figure 1: Time evolution of the 2D transient heat diffusion solution. Parameters in Table 1.

where, E , ν , u_x , u_y refer to the elasticity modulus, poisson's ratio and displacement components along the respective x and y directions.

The corresponding set of discrete element equations can be given in the form of a matrix assembly as,

$$\begin{aligned} \mathbf{K}\mathbf{r} &= \mathbf{F} \\ \mathbf{K} &= \int \mathbf{B}^T \mathbf{D} \mathbf{B} \, dx dy \\ \mathbf{F} &= \left[-\int \mathbf{N}^T t_x dS \right. \\ &\quad \left. -\int \mathbf{N}^T t_y dS \right] \end{aligned} \tag{7}$$

where, t_x , t_y refer to the applied traction forces along the surface of the boundary domain, while \mathbf{r} refers to the displacement vector.

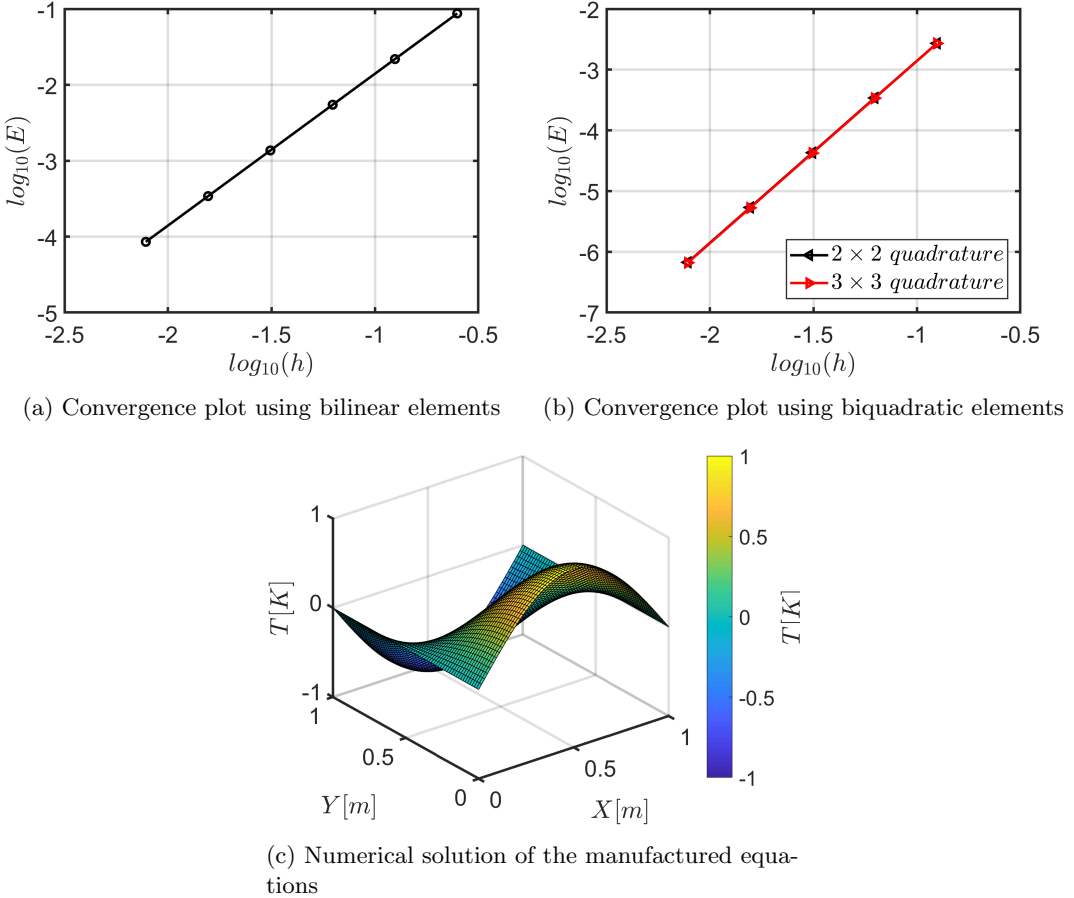


Figure 2: Code verification for the 2D diffusion equation.

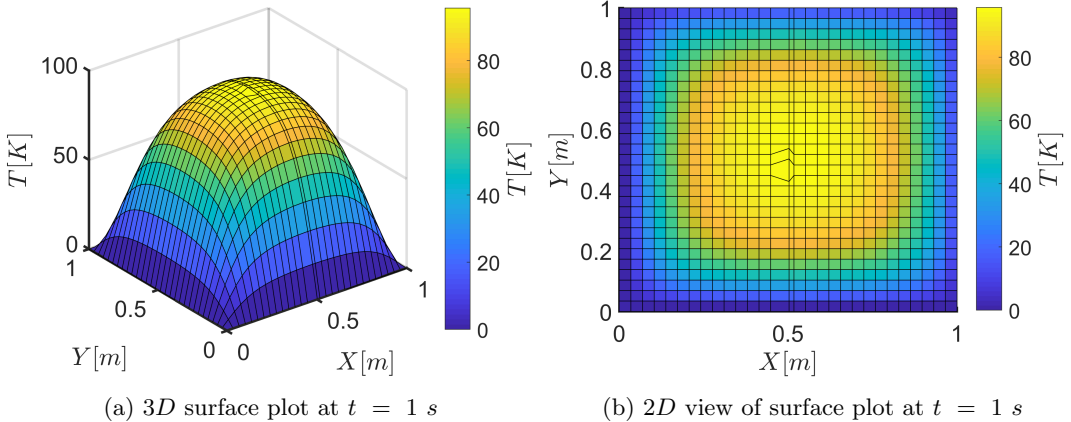


Figure 3: Test to verify working of the code during grid deformation. Near the domain center, the grid is slightly perturbed by 0.02 m.

To test the code framework in handling solid mechanics problems, a pure shear setup was simulated, where shear was applied at the top of the domain. Accordingly, a non-zero dirichlet x displacement boundary condition was imposed at the top boundary, while zero dirichlet boundary conditions were imposed for both x, y displacements at the bottom boundary. Additionally, the left and right boundaries were kept free, with no boundary conditions explicitly enforced. Due to the nature of these boundary conditions, the traction force terms in Eqn. 7 were ignored. In the numerical setup, no transient time stepping scheme was employed unlike the 2D transient diffusion problem. In other words, the displacements from the FEM solution were used to update the coordinates of the mesh in just one step,

Parametric variables	Parameters
Domain lengths	1 m (both x & y)
Elements	32 (both x & y)
Young's modulus	10^5 Pa
Poisson's ratio	0.49

Table 2: Parameters used for simulating 2D elasticity equation

thus resulting in a sheared mesh configuration. The list of parameters used for this study are detailed in Table 2, and the corresponding mesh configuration before and after the shear shown in the Fig. 4. Overall, the sheared mesh and the deformation near the corners is in good agreement with the results shown in [1, 2]. As done in 2D transient diffusion problem, the credibility of the results were again verified here by using both bilinear and biquadratic elements with 2×2 and 3×3 Gauss quadrature points.

Successful code verification of this setup was also performed by using the method of manufactured solutions. For this purpose, the manufactured x and y displacement components were respectively chosen to be $\sin(x) \cos(y)$ and $\cos(x) \sin(y)$. Substituting these expressions into Eqn. 7 respectively yielded $-\frac{E}{(1+\nu)(1-2\nu)}(2\nu-2)\sin(x)\cos(y)$ and $-\frac{E}{(1+\nu)(1-2\nu)}(2\nu-2)\sin(y)\cos(x)$ as the right hand side terms, which need to be accounted as boundary conditions in the assembly matrix (Eqn. 7). Using bilinear shape functions and 2×2 gauss legendre quadrature integration points, an order of accuracy equal to 2.0032 was obtained. Additionally, biquadratic shape functions and 3×3 gauss quadrature points yielded an order of accuracy equal to 3.0603. The obtained convergence plot and the corresponding mesh setup on using these manufactured equations are shown in Fig. 5. The L_2 convergence errors plotted in Fig. 5 were computed in the form of $\sqrt{\int [(u_{x,fem} - u_{x,mms})^2 + (u_{y,fem} - u_{y,mms})^2] dV}$, where the subscripts *fem* and *mms* respectively refer to the current FEM solution and manufactured equations. The computed order of accuracy is consistent with the expected order of accuracy on using bilinear and biquadratic shape functions, which deems the current code framework to be reliable for subsequent simulations.

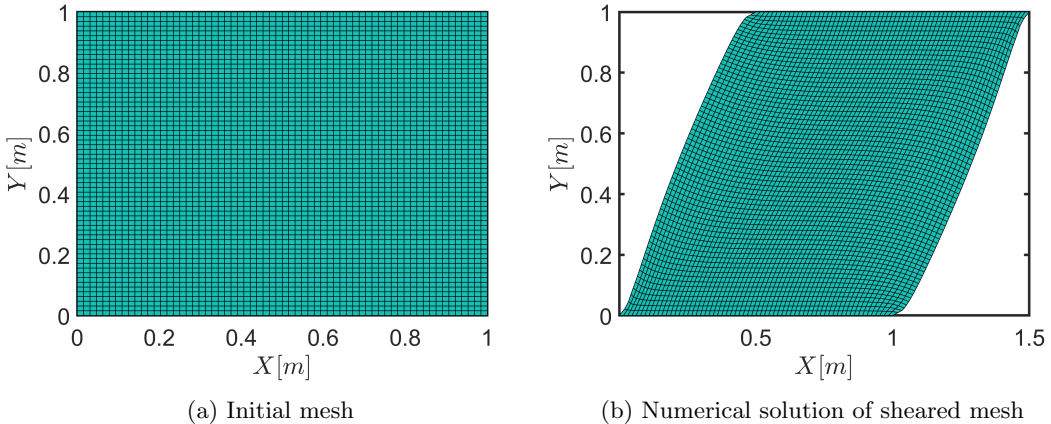


Figure 4: Snapshot of the initial and sheared mesh configuration for a pure shear setup. Parameters in Table 2.

3 2D dam break flow (Stokes equation)

This section studies a two-dimensional stokes flow equation, and the conservation equations include the continuity and momentum equations (a simplified form of the Navier-Stokes equations),

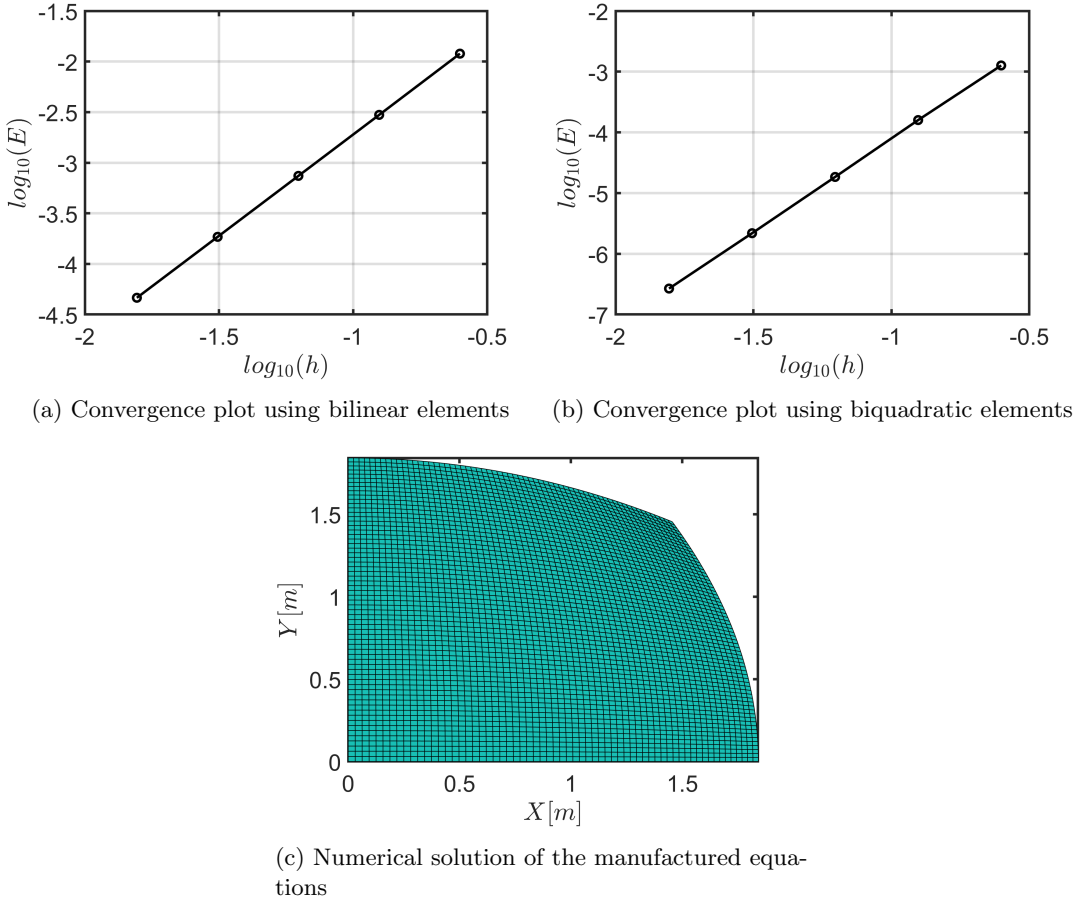


Figure 5: Code verification for the 2D elasticity equation.

$$\begin{aligned}
 -\frac{\partial p}{\partial x} + \frac{\partial}{\partial x} \left(2\eta \frac{\partial u_x}{\partial x} \right) + \frac{\partial}{\partial y} \left(\eta \left(\frac{\partial u_x}{\partial y} + \frac{\partial u_y}{\partial x} \right) \right) &= 0 \\
 -\frac{\partial p}{\partial y} + \frac{\partial}{\partial y} \left(2\eta \frac{\partial u_y}{\partial y} \right) + \frac{\partial}{\partial x} \left(\eta \left(\frac{\partial u_x}{\partial y} + \frac{\partial u_y}{\partial x} \right) \right) &= \rho g \\
 \frac{\partial u_x}{\partial x} + \frac{\partial u_y}{\partial y} &= 0
 \end{aligned} \tag{8}$$

These equations can be rewritten in a similar form as done in 2D elasticity equation (using the constitutive relations for describing viscous fluids, and relation between stresses and displacements),

$$\begin{aligned}
 \mathbf{B}^T \mathbf{D} \mathbf{B} \mathbf{u} - \mathbf{B}^T (\mathbf{m} p) &= \mathbf{F} \\
 \mathbf{m}^T \mathbf{B} \mathbf{u} &= 0
 \end{aligned} \tag{9}$$

where, the \mathbf{B} matrix is the same as defined in Eqn. 6. \mathbf{u} , p refer to the velocity vector and pressure respectively. The matrices \mathbf{m} and \mathbf{D} can be given as,

$$\begin{aligned}
 \mathbf{m} &= \begin{bmatrix} 1 \\ 1 \\ 0 \end{bmatrix} \\
 \mathbf{D} &= \begin{bmatrix} 2\eta & 0 & 0 \\ 0 & 2\eta & 0 \\ 0 & 0 & 2\eta \end{bmatrix}
 \end{aligned} \tag{10}$$

The corresponding set of discrete element equations can be given in the form of a matrix assembly as,

Parametric variables	Parameters
Domain lengths	1 m (both x & y)
Elements	20 (both x & y)
Viscosity	1 m ² /s
Source term (gravity)	1 (along -y)

Table 3: Parameters used for simulating 2D dam break flow

$$\begin{bmatrix} \mathbf{K} & \mathbf{G} \\ \mathbf{G}^T & \mathbf{0} \end{bmatrix} \begin{bmatrix} \mathbf{U} \\ \mathbf{p} \end{bmatrix} = \begin{bmatrix} \mathbf{F} \\ \mathbf{0} \end{bmatrix} \quad (11)$$

where,

$$\begin{aligned} \mathbf{K} &= \int \mathbf{B}^T \mathbf{D} \mathbf{B} dV \\ \mathbf{G} &= - \int \mathbf{B}^T \mathbf{m} \mathbf{N}_p dV \\ \mathbf{F} &= - \int \begin{bmatrix} \mathbf{N}^T F_x \\ \mathbf{N}^T F_y \end{bmatrix} dV + \int \begin{bmatrix} \mathbf{N}^T t_x \\ \mathbf{N}^T t_y \end{bmatrix} dS \end{aligned} \quad (12)$$

where, \mathbf{N} , \mathbf{N}_p refer to the shape functions used for describing the velocities and pressure respectively.

To test the code framework in handling stokes flow problems, transient flow in a dam break was simulated. To avoid any instabilities due to the coupling between pressure and velocity components, biquadratic and bilinear shape functions were used for describing the velocity and pressure respectively, along with 3×3 Gauss quadrature integration points. Normal velocity components along the left and bottom boundary were imposed to be of zero dirichlet type, while others were left free, without imposing any explicit boundary conditions. Additionally, a source term resembling the gravity force in the vertically downward (y) direction was imposed. For simplicity, time evolution was performed here by mere advection of the grid with the displacement at every time step (product of velocity and time step). A much robust way of handling advection will be discussed in the next section concerning viscous fingering instability. Due to the nature of these boundary conditions, the traction force terms were ignored. Fig. 6 shows the time evolution of the fluid (corresponding parameters in Table 3), where the fluid tries to settle at the bottom surface of the domain once the dam breaks. Due to the simplicity of the advection scheme employed here, topological changes of the mesh deformation (like splashing of water when it hits the surface) cannot be unfortunately simulated here. Advanced numerical schemes like Smoothed particle hydrodynamics (SPH), volume of fluid methods, interface tracking etc. may be the need of hour if such complex phenomena need to be captured.

4 Viscous fingering in porous media

As a next step, the current section studies viscous fingering instabilities (also commonly termed as Saffmann taylor instabilities) which arises when two viscous moving fluids (solvent and oil) try to displace one another in a porous medium.

The coupled conservation equations for this problem comprise of the continuity, Darcy and advection-diffusion equations for the solvent concentration respectively,

$$\begin{aligned} \nabla \cdot \mathbf{u} &= 0 \\ \mathbf{u} &= -\frac{k}{\mu(c)} \nabla p \\ \phi \frac{\partial c}{\partial t} + \nabla \cdot (\mathbf{u} c) &= \nabla \cdot (k \nabla c) \\ \mu(c) &= \left(\frac{c}{\mu_s^{1/4}} + \frac{1-c}{\mu_o^{1/4}} \right) \end{aligned} \quad (13)$$

where \mathbf{u} , k , $\mu(c)$, p , ϕ , c , μ_s , μ_o refer to the velocity vector, permeability, bulk mixture velocity, pressure, porosity, solvent concentration and viscosities of solvent and oil respectively. From these

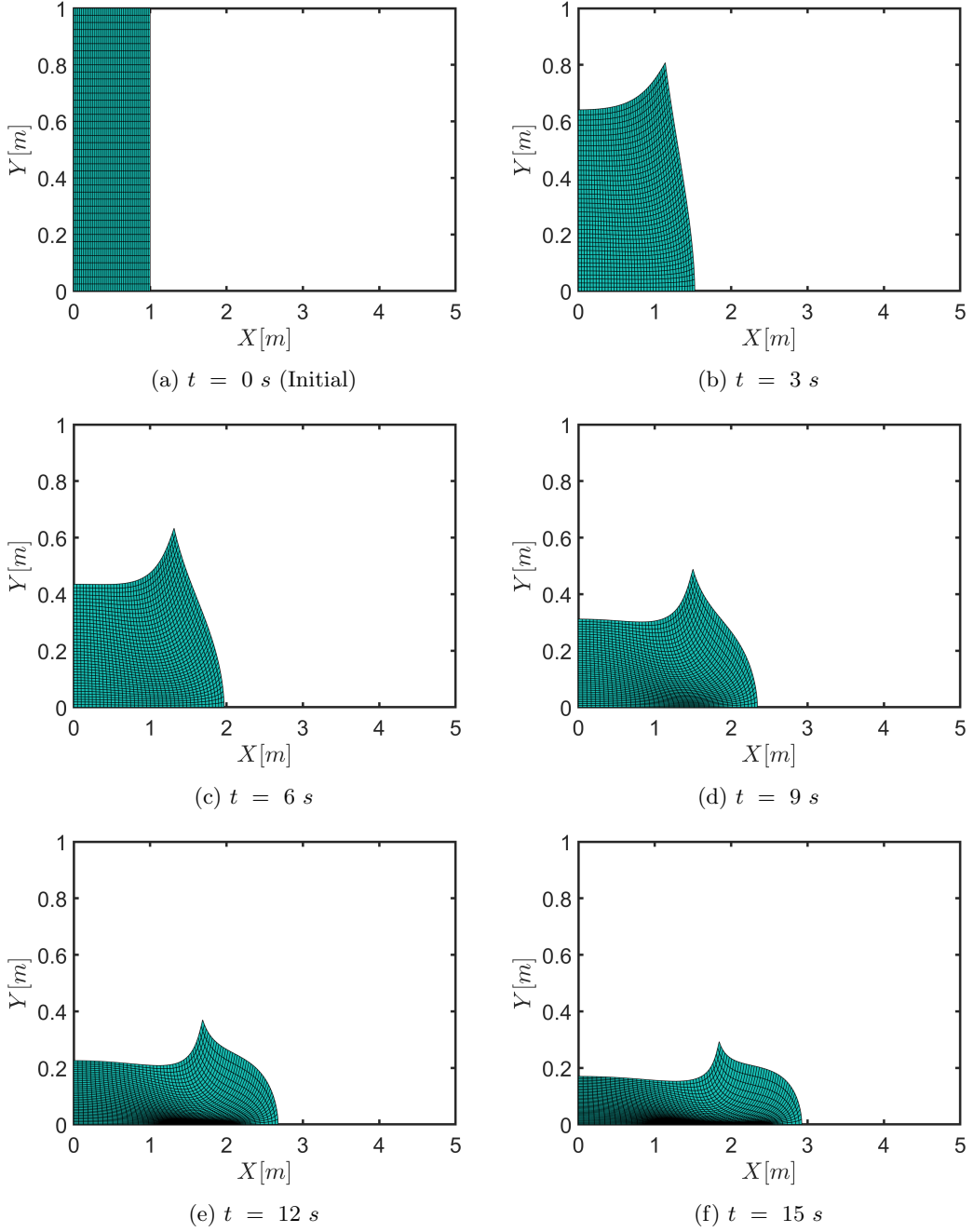


Figure 6: Time evolution of the 2D dam break flow problem. Parameters in Table 3.

equations, it can be noticed that unlike the Stokes flow problem, pressure and velocity flow variables here are coupled, and need not be separately solved for. Since this problem is highly advection dominated resulting in a hyperbolic PDE, stable solutions were obtained here by employing a variant of Galerkin FEM, known as Petrov-Galerkin FEM.

Using the Petrov-Galerkin method (analogous to upwind schemes in finite volumes and finite differences) for solving the advection part, the weighting functions were appropriately varied as a function of the Peclet number (Pe). These can be given by [3],

Parametric variables	Parameters
Domain lengths	10 m (both x & y)
Permeability	$10^{-13} \text{ m}^2/\text{s}$
Porosity	0.1
Solvent diffusivity	$10^{-9} \text{ m}^2/\text{s}$
Solvent viscosity	$1.33 \times 10^{-4} \text{ Pas}$
Oil viscosity	$2.66 \times 10^{-3} \text{ Pas}$
Elements	20 (both x & y)
Time step	$10^{-4} \text{ secs/year}$

Table 4: Parameters used for simulating viscous fingering instability phenomenon (Fig. 7).

$$\begin{aligned}
W_i &= N_i + \frac{\alpha h}{2} \frac{u_j}{|\mathbf{u}|} \frac{\partial N_i}{x_j} \\
\alpha &= \coth(Pe) - \frac{1}{Pe} \\
Pe &= \frac{|\mathbf{u}| \delta x}{2k}
\end{aligned} \tag{14}$$

where δx refers to the elemental grid spacing.

The discrete element equations in the form of an assembled matrix can be given as,

$$\begin{bmatrix} \mathbf{K}\mathbf{P}(c) & 0 \\ 0 & \frac{\mathbf{M}\mathbf{M}}{\delta t} + \mathbf{C}\mathbf{M} + \mathbf{K}\mathbf{M} \end{bmatrix} \begin{bmatrix} \mathbf{p}^{n+1} \\ \mathbf{c}^{n+1} \end{bmatrix} = \begin{bmatrix} 0 & 0 \\ 0 & \frac{\mathbf{M}\mathbf{M}}{\delta t} \end{bmatrix} \begin{bmatrix} \mathbf{p}^n \\ \mathbf{c}^n \end{bmatrix} \tag{15}$$

and the respective matrices in the above assembly are,

$$\begin{aligned}
\mathbf{M}\mathbf{M} &= \int \int \phi \mathbf{W}^T \mathbf{N} dx dy \\
\mathbf{C}\mathbf{M} &= \int \int \left(u_x \mathbf{W}^T \frac{\partial \mathbf{N}}{\partial x} + u_y \mathbf{W}^T \frac{\partial \mathbf{N}}{\partial y} \right) dx dy \\
\mathbf{K}\mathbf{W} &= \int \int k (\nabla \mathbf{N})^T \nabla \mathbf{N} dx dy \\
\mathbf{K}\mathbf{P}(c) &= \int \int \frac{k}{\mu(c)} (\nabla \mathbf{N})^T \nabla \mathbf{N} dx dy
\end{aligned} \tag{16}$$

As seen in the assembly matrix, the advection term is discretized with a first order implicit approach. Unlike the Stokes flow problem, biquadratic shape functions were used for both pressure and solvent concentration, which does not report any instabilities. As an initial condition, small random perturbations were induced in the solvent concentration. Additionally, dirichlet pressure boundary conditions were imposed on the left side, while other boundaries kept free. Table 4 details the list of parameters adopted for the numerical simulation results shown in Fig. 7.

Acknowledgements

I would like to thank the course instructors, Dr. Antoine Rozel and Dr. Patrick Sanan for their help and guidance in the completion of the tasks detailed in this report.

References

- [1] U. Exner, M. Frehner, N.S. Mancktelow, and D. Grujic. Why homogeneous boundary conditions lead to heterogeneous internal strain in analogue simple shear experiments - explained by numerical modeling. EGU General Assembly, Vienna, Austria, ETH Zürich, 2010.
- [2] D. Grujic and N.S. Mancktelow. Folds with axes parallel to the extension direction: an experimental study. *Journal of Structural Geology*, 17(2):279 – 291, 1995.

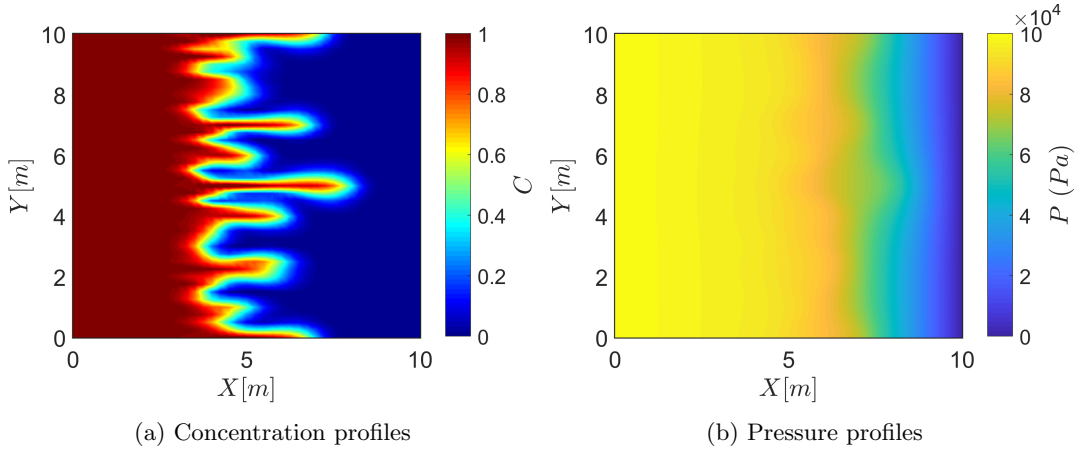


Figure 7: Snapshot of the viscous fingering instability in porous media after 110 time steps. Parameters in Table 4

- [3] O.C. Zienkiewicz and R.L. Taylor. *Finite Element Method: Vol. 3: Fluid Dynamics*. Elsevier Science & Technology Books, 2000.
- [4] G. Simpson. *Practical finite element modeling in earth science using matlab*. Wiley Online Library, 2017.
- [5] A. Rozel and P. Sanan. Lecture notes in introduction to finite element modeling in geosciences, Spring semester 2019.